

First results from Mexnext:

Analysis of detailed aerodynamic measurements on a 4.5 m diameter rotor placed in the large German Dutch Wind Tunnel DNW

J.G. Schepers, ECN
L. Pascal, SupAero - ISAE
H. Snel, ECN

Paper presented at the European Wind Energy Conference and Exhibition (EWEC), April 20-23, 2010, Warsaw, Poland

ECN-M--10-045 June, 2010

First results from Mexnext: Analysis of detailed aerodynamic measurements on a 4.5 m diameter rotor placed in the large German Dutch Wind Tunnel DNW

J.G. Schepers
The Energy Research Centre of the Netherlands
schepers@ecn.nl

L.Pascal

SupAero - ISAE (Institut Superieur de l Aeronautique et de l Espace) lucas.pascal@gmail.com

H. Snel
The Energy Research Centre of the Netherlands
snel@ecn.nl

1 Abstract

This paper presents an analysis of measurements which have been taken in the EU project Mexico (Model Rotor Experiments In Controlled Conditions). In the Mexico project a large number of European research institutes and universities cooperated. The project resulted in a database of measurements on a 3 bladed 4.5 m diameter wind turbine model placed in the LLF tunnel (with a 9.5 by 9.5 m² open test section) of DNW in the Netherlands. Pressure and load measurements on the blade have been carried out simultaneously with stereo PIV flow field measurements.

An extensive analysis of the Mexico measurements takes place within IEA Task 29 Mexnext. The paper presents recent results from ECN obtained within the framework of this IEA Task where special attention is paid to the correlation between pressure measurements and the overall wind turbine loads, the influence of the rotational speed on the aerodynamics, the correlation between pressure measurements and the tip vortices in the wake, the non-uniformity of the flow within the rotor plane and the tip vortex trajectories at yawed conditions

Keywords: wind turbine aerodynamics, wind tunnel measurements,

2 Introduction

In the past the accuracy of wind turbine design models has been assessed in several validation projects, see e.g. [1]. They all showed that the modeling of a wind turbine response (i.e. the power or the loads) is subject to large uncertainties. These uncertainties mainly find their origin in the aerodynamic modeling, where several phenomena, like 3D geometric and rotational effects, instationary effects, yaw effects, stall, tower effects etc, contribute to unknown responses in particular at off-design conditions. The availability of high quality measurements is considered to be the most important pre-requisite to gain insight into these uncertainties and to validate and improve aerodynamic wind turbine models. For this reason the



Figure 1: LLF (Large Scale Low Speed Facility) of DNW (German Dutch Wind Tunnel) (Picture from http://www.twanetwerk.nl)

European Union project Mexico (Model Rotor Experiments In Controlled Conditions) has been carried out. In this project 10 institutes from 6 countries cooperated in doing experiments on an in-

strumented, 3 bladed wind turbine of 4.5 m diameter placed in the 9.5 by 9.5m² open section of the Large Low-speed Facility (LLF) of DNW in the Netherlands. The measurements were performed in December 2006 and resulted in a database of combined blade pressure distributions, loads and flow field measurements, which can be used for aerodynamic model validation and improvement. Previous measurements (on a 10 m diameter turbine) were performed by NREL in the NASA Ames wind tunnel, [2]. An obvious difference between the two types of experiments lies in the larger size of the NASA-Ames experiment but on the other hand the NASA-Ames experiment only contained rotor measurements where the Mexico experiment also included extensive flow field measurements using the stereo PIV technique. Furthermore the Mexico model is three bladed, whereas the NREL model was two bladed. Finally, the majority of the NREL measurements concern stalled flow, while the entire operational envelope is covered in the Mexico measurements.

A thorough analysis of the Mexico data (also in comparison with the results obtained from the NASA-Ames experiment) is performed within IEA Wind Task 29 Mexnext (www.mexnext.org) coordinated by ECN. In Mexnext, 17 parties from 11 different countries participate. The present paper reports recent analyses carried out by ECN.

It is noted that the results as presented in this paper have not been corrected for tunnel effects. As a matter of fact CFD calculations from [3] indicate these effects to be small at design conditions, due to the open jet configuration. It is acknowledged however that tunnel effects are expected to be more severe at high loading and at yawed flow. For this reason a more thorough thorough study of tunnel effects will be carried out within Mexnext.

In the sequel of this paper the azimuth angle is defined such that 0 degrees corresponds to the 12 o clock position and 270 degrees is at the 9 o clock position (the Mexico rotor rotates clock-wise). A horizontal x-y coordinate system is used, see figure 13, with the x-coordinate along the tunnel velocity direction (x=0 in the rotor plane) and the y-coordinate is oriented outboard in radial direction at the 9 o clock position (y=0 in the rotor centre).

3 Experimental set-up and data collected

The LLF facility of DNW is shown in figure 1 where the setup of the Mexico experiment is given in figure 2. The turbine is placed in the 9.5x9.5m² open jet configuration with a measurement section of 20 meter length. The rotor plane of the turbine is lo-

cated 7 meter downstream of the nozzle and 13 meter upstream of the collector.



Figure 2: Setup of model turbine in the Measurement Section of the DNW LLF

The external six component balance is the blue structure beneath the model in figure 2. This balance recorded the total rotor loads statically. The (twisted, tapered) rotor blades were numerically milled from aluminum, to ensure (within strict tolerances) identical shapes.

Pressure distributions on the blades were obtained from 148 Kulite absolute pressure sensors, distributed over 5 sections at 25, 35, 60, 82 and 92% radial position respectively. Three different aerodynamic profiles (DU91-W2-250, RISØ-A1-21 and NACA 64-418) were used in the design. The DU91-W2-250 airfoil was applied from 20 to 45.6% span, the RISØ-A1-21 airfoil from 54.4% to 65.6% span and the NACA 64-418 airfoil outboard of 74.4% span. Hence a constant airfoil is applied over a considerable radial extension around the instrumented sections in order to assure known conditions at each of these sections, where the remaining length is used for the transition from 1 airfoil to another. Blade loads were monitored through two strain-gauge bridges at each blade root. Pressures and strains were sampled at 5.5 kHz. The rotational speed was either 424.5 rpm or 324.5 rpm. Note that, unless otherwise stated, the results presented in this paper have been taken at 424.5 rpm. At 424.5 rpm a chord based Reynolds number of approximately 0.8 M was reached without entering into noticeable compressible conditions; the blades were tripped to avoid possible laminar separation phenomena. Pressure and load measurements were done at different tunnel speeds (denoted with V_{∞}) ranging from 10 m/s to 30 m/s, yielding tip speed ratios (denoted with λ) between 3.3 and 10. Note that the design tip speed ratio is 6.67, which corresponds to V_{∞} = 15 m/s at 424.5 rpm. Different yaw angles (denoted with β) and pitch angles were covered, including the design pitch angle of -2.3 degrees.

Extensive flow field mapping of the three velocity components has been done by DNW with stereo PIV measurements. The flow field measurements were combined with measurements of the pressures and the blade root moments. The PIV measurements were performed in the following way:

- A traversing tower with two cameras focusses on a PIV sheet with a size of 337*394 mm². The PIV sheet is located horizontally in the symmetry plane of the rotor at the 270 degrees azimuth position, see figure 3. The PIV tower is moveable in the horizontal x-y direction;
- The flow field is seeded with small bubbles which are brought into the settling chamber, upstream of rotor;
- The seeded PIV sheet is illuminated with a strong laser flash, and two digital photographs are taken with a delay of 200 nanoseconds and a comparison is made between the two seeding fields:
- The PIV sheet is then subdivided into small interrogation windows (with a size of 4.3x4.3 mm²) and a large number of velocity vector fields are attempted. The actual velocity vector of the interrogation window is the one resulting in maximum cross correlation between the two seeding fields.

The PIV samples were taken rotor-phase locked with a frequency of 2.4 Hz. Each PIV data point consists of several (30-100) samples. Although all individual samples are stored, the present paper discusses the averaged results only.

The PIV flow field measurements are done at both non-yawed and yawed flow:

- \circ Non-yawed measurements are performed at V_{∞} = 10, 15 and 24 m/s, a rotor speed of 424.5 rpm and different pitch angles (the present paper only discusses measurements at the design pitch angle of -2.3 degrees). The following type of experiments are carried out:
 - Two radial PIV traverses from y/R = 0.52 to y/R = 1.22 where an overall axial range is covered from x = -0.13R to x = +0.13R. The two traverse have a small overlap in the rotor plane, see figure 4. The radial traverses are performed at 6 blade azimuth positions with a 20 degrees azimuth interval (where the 3P flow dependancy makes it sufficient to cover only 120 degrees azimuth).
 - \circ Two axial traverses at y/R = 0.61 and y/R = 0.82 from x = -4.5 m to x = 5.9 m (i.e. from 1.D upstream of the rotor to 1.31 D downstream of the rotor). Note that the y-locations refer to the centres of the PIV sheet. The azimuthal position of blade 1 (denoted with Ψ) was 0 de-

grees;

- Tip vortex tracking experiments in which the position of the tip vortex is searched by trial and error. The position of blade 3 was 270 degrees.
- Yawed measurements have been performed at yaw angles of plus and minus 30 degrees and a tunnel speed of 15 m/s, where the pitch angle = -2.3 degrees. Both axial and radial traverses have been performed in a procedure very comparable to the procedure as described at aligned conditions. The locations of the PIV sheets were also more or less similar. Furthermore a vortex search has been carried out. In view of the fact that the PIV sheets were located in the horizontal symmetry plane at an azimuth angle of 270 degrees, the measurements at the plus and minus yaw angle represent the flow field at two opposite azimuth angles (90 and 270 degrees) for the same vaw angle. Note that this is strictly spoken not fully true since the wake rotation remains counterclockwise independant of the sign of the yaw angle. It is expected however that the effect of the wake rotation on the subjects discussed in the present paper is limited.

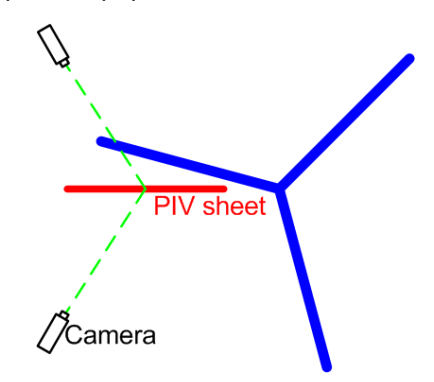


Figure 3: Location of blade position and PIV sheet

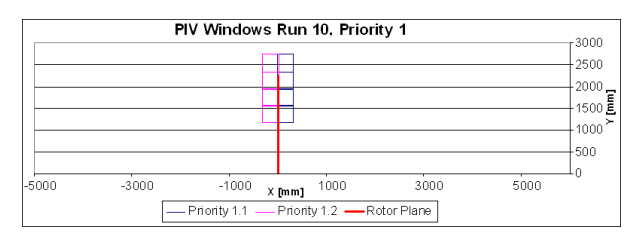


Figure 4: PIV measurement sheets at radial traverses as seen from above

4 Results

Previous results of analyses have been described in [4] and [5]. Most of the present analyses focuses on new studies, in particular:

 The correlation between pressure measurements along the blade and the tower foot loads as measured with the DNW balance, section 4.1.

- The influence of rotational speed on the aerodynamics of a wind turbine, section 4.1.
- The blade bound vortex strength as derived from the pressure measurements in relation to the strength of the tip vortices as derived from the PIV measurements, section 4.2.
- The understanding of the flow field in and near the rotor plane, section 4.4
- The understanding of the flow field and tip vortex trajectories at yawed flow in comparison to CFD calculations and in comparison with the speed decay as analysed at non-yawed conditions, section 4.5

Note that section 4.3 repeats some results from [5], i.e. the velocity decay in axial direction at non-yawed conditions, which serves as a reference for the velocity decay at yawed conditions, as analysed in section 4.5.

4.1 Correlation between pressure and balance measurements and in uence of rotational speed

As described in section 3, pressure measurements are done at 25%, 35% 60%, 80% and 92% span. The resulting forces in axial and inplane direction are determined and integrated to the rotor axial force and torque, assuming a linear behaviour of the forces between the different sections, see figure 5.

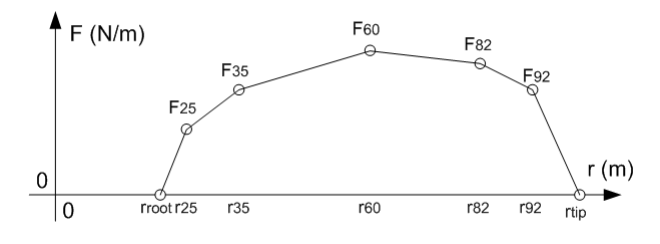


Figure 5: Assumed load distribution between the instrumented sections

In figure 6 the resulting axial force is compared with the axial force as measured with the balance and calculated with ECN's BOT program [6], which is a program based on the blade element momentum theory. It is noted that figure 6 presents the axial force on the rotor only, where the balance measurements at the foot of the tower also include the tower drag. The tower drag has been derived from the tower bottom moment and the tower bottom force, where the drag is assumed to be uniformly distributed over the (cylindrical) tower.

The axial force is divided by the square of the tun-

nel speed and presented as function of tip speed ratio. As such figure 6 represents the axial force coefficient (apart from the division through the constant air density and rotor area) as function of tip speed ratio. The results are given for the two rotational speeds 324.5 and 424.5 rpm. The presentation of force coefficient versus tip speed ratio is expected to make the results independent of the rotational speed, apart from a possible influence of Reynolds number and/or rotational (3D) effects on the airfoil data. It is then interesting to note that figure 6 shows these influences to be very small. This is consistent to later analyses in Mexnext where the influence of the rotational speed on the local aerodynamic profile coefficients (i.e. c_n and c_t) was found to be small. These results will be published in future literature. The very good agreement between the pressure and balance axial force is also interesting and gives confidence in both the pressure measurements as well as the axial force measurements from the balance.

The BEM code overpredicts the axial force. It is noted that within the Mexnext project results from several calculational codes (including full CFD methods) are compared with the Mexico measurements and many of them also overpredict the axial force for unknown reasons. These results will be reported in future literature.

The corresponding results of the torque (not presented in this paper) showed the influence of rotational speed on the torque coefficent as function of tip speed ratio to be limited in agreement with the observations on the axial force coefficient. The agreement between the torque from the pressure measurements and the balance torque was poor. This is due to the inaccuracies in the integration of the pressures to the inplane forces (the limited number of pressure taps makes a relatively large inaccuracy in inplane force inevatible) but futhermore an unsolved quality problem occurs in the torque as measured from the balance.

4.2 Blade circulation compared with tip vortex strength

In this section the bound vortex strength along the blade (blade circulation) is determined from the pressure measurements. This blade circulation is compared with the tip vortex strength as derived from the PIV measurements.

The bound vortex strength along the blade is determined from the Joukowsky theorem.

$$\Gamma = \frac{F_L}{\rho . V}$$

Where F_L is the lift force per unit length which is found from integration of the pressure distribution

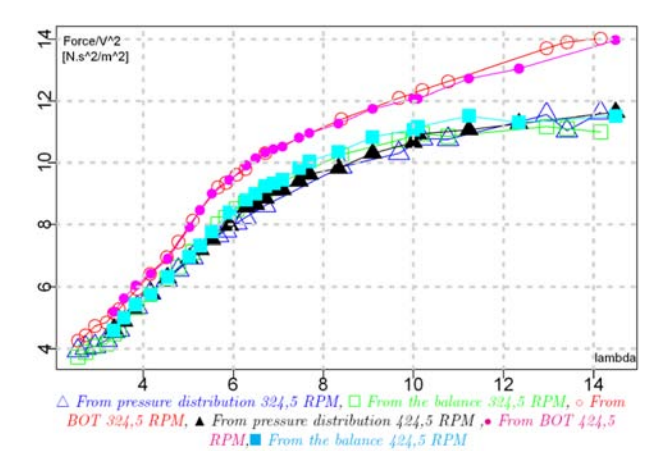


Figure 6: Comparison of axial force derived from pressure measurements, balance measurements and BOT (i.e. BEM) calculations for two different tip speeds

over the chord and V is the velocity at the blade section, where the induction in the rotor plane is derived from the PIV flow field measurements, see section 4.3, by assuming it to be half the induction at the most downstream position, in agreement with momentum theory.

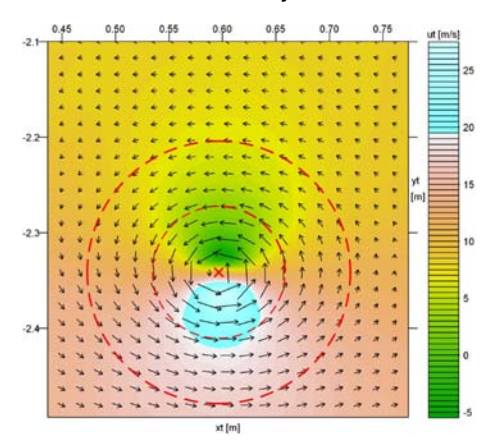


Figure 7: Measured velocity field containing a tip vortex. The circles were used for the integration to vortex strength

The tip vortex strength in the wake is found from the integral:

$$\Gamma = \oint \vec{V} \vec{ds}$$

along circles of different radii in the flow field, see figure 7. In figure 8 the tip vortex strength at different wake positions is given as function of integration radius for the design condition ($\lambda = 6.67$ i.e. $V_{\infty} = 15$ m/s). It can be seen that the tip vortex strength reaches an asymptotic value with increasing integration radius. Also indicated is the maximum bound vortex strength along the blade.

The maximum vortex strength for these conditions occurs at 35% span but as a matter of fact it varied only between 3.73 to 4.1 m²/s (with the exception of the 92% station where the bound vortex strength, due to tip effects is lower (3.58 m²/s)).

Such (almost) constant bound vortex strength is expected at the present (design) conditions since it goes together with a constant induction along the entire blade which was one of the design targets for the Mexico blade.

It is furthermore interesting to see a good agreement between the asymptotic value of the tip vortex strength in figure 8 and the bound vortex strength which indicates a very good correlation between the results from these two very different types of measurements (pressure measurements and PIV measurements).

Similar studies have been done at $\lambda = 4.17$ and $\lambda = 10.0$ (not presented in this paper). At these conditions a much stronger variation in bound vortex strength along the blade is found. This could be expected from the fact that these measurements are done at off-design conditions. Nevertheless the bound vortex strength at 82% span still compares well with the tip vortex strength.

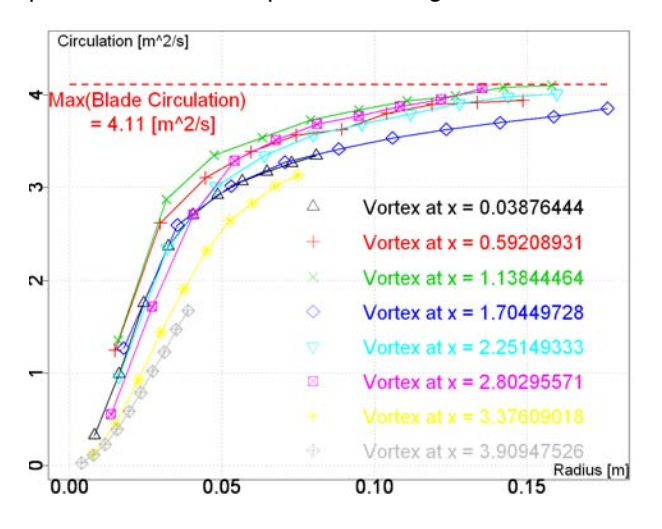


Figure 8: Tip vortex strength as function of integration radius for different x-positions in the wake. Also indicated is the maximum blade circulation

4.3 Axial velocity decay (non-yawed conditions)

In figure 9 the axial velocity decay at non-yawed conditions and different rotor loadings (λ = 4.17 (V_{∞} =24 m/s), λ = 6.67 (V_{∞} = 15 m/s), and λ = 10.0 (V_{∞} = 10 m/s)) are presented at 61% and 82% span. These measurements are done at a blade position of 0 degrees in a phase locked way. The results are averaged over the axial extent of

the PIV sheet.

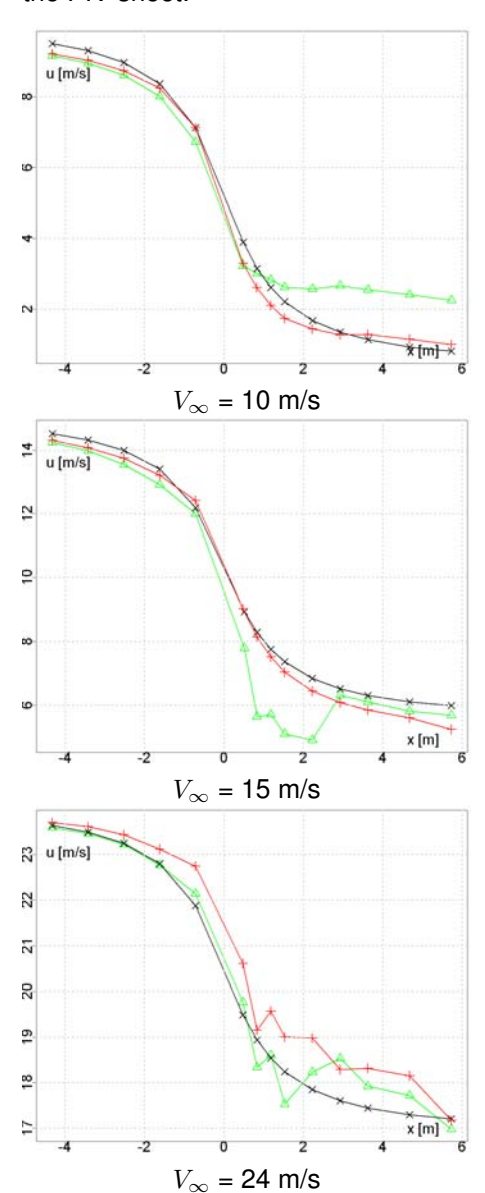


Figure 9: axial velocity decay at V_{∞} 10,15 and 24 m/s

Y = 1,374m (61% span),Y = 1,845m (82% span),

Cylindrical vortex wake method

Also indicated are the results from a cylindrical vortex wake method [7]. This model is based on an actuator disc approach with a constant bound vortex strength over the rotor plane which yields $\mathrm{C}_{\mathrm{Dax}}=4a(1\text{-}a)$ and $a_{\infty}=2~a_{\mathrm{rotor}},$ consistent to the results from the momentum theory.

At λ = 10 (which corresponds to $C_{\mathrm{D.ax}} \approx$ 1.0) a very strong deceleration of the wake flow is found from V_{∞} = 10 m/s to V < 1 m/s at x = 5.9 m and 82% span. The conditions are very close to the so-called turbulent wake state where momentum theory breaks down and where back flow in the wake could be expected. The present measure-

ments indicate very low, but positive, velocities with a smooth flow although there is still a deceleration at the most downstream position.

At λ = 4.17 (V_{∞} = 24 m/s), the blades are stalled (This could be confirmed by the pressure measurements) and the velocity decays show a more chaotic behaviour which is a result of vortex shedding from the stalled boundary layer into the wake.

At $\lambda=6.67~(V_\infty=15~m/s,$ i.e. design conditions) the axial velocity decay downstream of the rotor at 60% span is striking in the sense that velocity fluctuations appear near the rotor plane. These are most likely a result of the transition from the DU airfoil to the RISO airfoil, leading to a change in bound vortex strength near this location. It is interesting to note that CFD calculations, though they do predict a small change in bound vortex strength at that location have not been able yet to predict the velocity fluctuations as found in the measurements, see eg [5].

Generally speaking a good agreement is found between the measured decay and the decay from the cylindrical vortex wake model. This is in particular true at the locations upstream of the rotor plane and in the far wake. The discrepancies near the rotor plane are partly explained by the actuator disc assumption in the cylindrical vortex wake model which implies a uniform flow in the rotor plane, opposite to the real flow field situation, where the finite number of blade yields a strong non-uniformity, see section 4.4. Moreover the velocity fluctuations due to stall cannot be reproduced in the cylindrical vortex wake model, since this model does not include stall. Also the velocity fluctuations at 61% span and V_{∞} = 15 m/s due to the transition in airfoils cannot be reproduced since the model assumes a constant bound vortex strength along the blade.

The cylindrical vortex wake model implicitly assumes a constant velocity in radial direction. This assumption is to some extend confirmed by the present measurements, in particular at the locations upstream of the rotor and in the far wake. An exception is found in the results at $V_{\infty}=10~\text{m/s}$ where the velocity in the far wake and at 82% span is predicted well but the velocity at 61% span is underpredicted. It is recalled that this measurement is done at a condition very close to the turbulent wake situation, which is an extreme case in the sense that the momentum theory (and the cylindrical vortex wake model) are expected to break down, going together with a large non-uniformity of the flow.

4.4 Flow measurements near the rotor plane

In figure 11 the axial velocities as measured in the radial traverses (see section 3) are presented as function of the x-direction for r/R = 80% , 92% and 120% and V_{∞} = 15 m/s (i.e. λ = 6.67). The different lines represent different blade azimuth positions, see figure 10.

At the outboard station (i.e. at 120% span) the velocity traverse V(x) shows a clear maximum, the magnitude and location of which depends on the blade azimuth position. This maximum velocity is induced by the tip vortex at the x-location where it crosses the horizontal plane, i.e. the position where the tip vortex is as close as possible to the PIV sheet, see figure 13. This figure shows the tip vortex to induce a positive x-velocity at outboard positions. The x-location where the tip vortex passes the PIV sheet depends on the tip vortex travel speed. In [5] the tip vortex tracking measurements have been analysed which resulted in a vortex travel speed in the order of 11.86 m/s, constant throughout the wake. As noted in [5] this is smaller than the often assumed averaged value of the free stream and wake velocity (which would give 12.5 m/s in the rotor plane based on V_{∞} = 15 m/s and an axial induction factor of 1/3). On basis of the present analysis, an even lower transport velocity of 11.2 m/s is found near the rotor plane (since the tip vortex has traveled from x = 0.0997 m at $\Psi = 40$ degrees to x= 0.2774m at Ψ = 80 degrees). It must be realised however that the maximum in the velocity traverse is very flat which makes it difficult to determine the precise location of the tip vortex and resulting vortex travel speed.

Figure 11 shows the maximum velocity at $\Psi=80$ degrees and 120% span to be larger than the velocity at $\Psi=60$ degrees. This is due to the fact that the relevant tip vortex at $\Psi=80$ degrees (which is trailed from blade 3 at 320 degrees azimuth) crosses the x-y plane at a more downstream position. Due to the wake expansion this goes together with a more outboard location, closer to the 120% span location.

At the 80% and 92% span a strong non-uniformity in the rotor plane can be observed with a jump in velocity when the blade moves from $\Psi=20$ to $\Psi=40$ degrees. Thereto it should be realised that $\Psi=20$ degrees corresponds to a position of blade 3 at 260 degrees i.e. just below the PIV sheet at 270 degrees azimuth where its bound vortex increases the axial velocity, see figure 12. At $\Psi=40$ degrees the blade is just above the PIV sheet and the bound vortex decreases the axial velocity. The jump in velocity at x=0 m is smaller at 92% span consistent with the observation from section 4.2 of a smaller

bound vortex strength at this location.

Also at the other blade positions the non-uniformity in the flow appears to be large: At 80% span and x=0 m, the velocity varies from V = 9.5 m/s at $\Psi =$ 60 degrees to V = 11.2 m/s at Ψ = 120 degrees. At 92% span, the velocity varies from V = 11 m/s at Ψ = 60 degrees to V = 12 m/s at Ψ = 120 degrees. As a matter of fact, at 92% span, the closer proximity to the discrete tip vortices (the phenomenum modelled with the Prandtl tip correction), was expected to give a stronger flow non-uniformity with a smaller local blade velocity. The present measurements however indicate the flow at 92% span to be slightly more uniform with a higher local blade velocity. This may be a result of the fact that the flow non-uniformity at 92% span is still dominated by the passage of the blade where the bound vortex strength at that position is weaker than at 82% span, as noted in section 4.2. The velocities induced by the tip vortex are visible in the form of a (relatively slight) minimum at those x-locations where the velocity at 120% span appears to be maximum (Note that the positive x-velocity as induced at positions outboard of the tip vortex, turns into a negative velocity at an inboard location). At 92% span the drop in velocity is however not very pronounced yet, despite the fact that the Prandtl tip correction factor at that location is calculated to be 0.825 (versus 0.97 at 80% span). Within Mexnext the flow field measurements at more outboard stations will be investigated together with detailed CFD analysis in order to shed more light on these phenomena.

Finally it is worthwile to note the multi-valued curves near x=0, which are a result of the overlapping PIV sheets at this position. The results are usually (but not always) very compatible indicating a good quality of the data. This is also confirmed by the (general) good compatability of the results at Ψ = 0 and 120 $^{\circ}$.

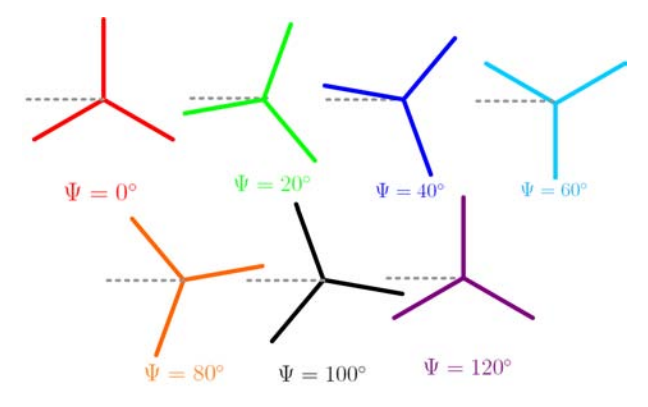


Figure 10: Position of blade 1 at Ψ = 0, 20, 40, 60, 80, 100, 120 $^{\circ}$

4.5 Flow eld and tip vortices at yaw

In figure 14 the tip vortex trajectories at +/- 30 degrees yaw (yaw angle indicated by β) are presented from the tip vortex tracking experiments. The blade position at these tip vortex tracking measurements was Ψ = 270 degrees. As stated before the measurements at negative yaw and 270 degrees azimuth are assumed to be representative for the results at positive yaw and 90 degrees azimuth.

Figure 14 shows the wake expansion at 90 degrees azimuth (i.e. at the so-called upwind side of the rotor plane) to be significantly different from the wake expansion at 270 degrees azimuth (i.e. at the downwind side of the rotor plane): At 90 degrees the initial expansion is limited (the tip vortices travel at a constant radial position of $r\approx 2.25\,$ m) where a strong expansion appears at 270 degrees azimuth.

These differences in expansion can be explained by the effect of the axial induced velocity on the wake skew angle (χ) , see eg [7]:

$$\tan \chi = \frac{V \sin \beta}{V \cos \beta - u_i} \tag{1}$$

with u_i is the axial induced velocity. As explained in [7] the induced velocity at the downwind side of the rotor plane is high leading to a strong wake expansion from equation 1. The opposite happens at the upwind side where the induced velocity is small.

The measurements from figure 14 have been reproduced with the Virtual Blade Model of the commercial CFD code Fluent, see figure 15 and [3]. The VBM model of Fluent is basically an actuator disc model and as such it does not capture the distinct tip vortices.

Both calculations and measurements show a strong wake expansion at the downwind side of the rotor plane, and, initially, a limited wake deflection at the upwind side. As explained before, this limited deflection was expected to be a result of the low induction but in addition the VBM calculations show the nacelle geometry as an important factor which avoids a wake deflection.

Hence the comparison between the results from figures 14 and 15 shows a very good qualitive agreement between the VBM predictions and the measured flow field. This is even more true if one realises that the axial velocity traverses (see below) indicate that for x> 3 m (the part of the flow not covered by the tip vortex tracking experiments), the wake is deflected downward in agreement with the results from the VBM model. Nevertheless a quantititive assessment of the VBM code

(eg in terms of a comparison between the tip vortex positions and the location of maximum vorticity) showed relatively large discrepancies, see [3].

Figure 16 shows the axial velocity as function of the axial coordinate at two radial positions (y = 1.374 m and y = 1.75 m (61% and 78% span). The corresponding results at zero yaw (as discussed in section 4.3) are also plotted. Note that results have been averaged over the axial extent of the PIV sheets where the zero velocity at 30 degrees yaw and x=2m, y = -1.374 m is a result of the nacelle being present at that position.

The axial traverses at positive yaw initially show a reduced velocity behind the rotor followed by an abrupt increase to the free stream velocity of ≈ 15 m/s. This rapid increase is visible at both radial stations but it happens at earlier x for the inner station. It can be explained by considering the tip vortex trajectories and the locations of the axial traverses. see figure 14. The PIV sheets at positive yaw are located at the upwind side of the rotor plane where figure 14 shows the initial wake expansion to be limited with the edge of the wake at $y \approx 2.25$ m. The axial traverses at y=1.374 m and y=1.75 m then remain within the wake with consequent lower velocities. However at larger x-locations the wake may be expected to deflect downward, see also the predictions from the Virtual Blade Model in figure 15, by which the traverse at y = 1.75 m crosses the edge of the wake and continues in the free stream where V = 15m/s. At an even further downstream location, when the wake edge is deflected to y < 1.375 m, the PIV traverse at the inner position will also cross the wake edge and the velocity will reach the free stream value.

The traverse at negative yaw corresponds to a traverse at the downwind side of the rotor plane. At this side figure 14 shows a wake expansion by which the entire traverse at both r=1.374 m and r=1.75 remains within the wake where the velocities are lower than the free stream velocities.

5 Conclusions

This paper discusses several results from the Mexico experiment.

- The effect of the rotational speed on the aerodynamic load coefficients was found to be small.
- The axial velocity decay is predicted reasonably well with a simple cylindrical vortex wake model but some deviations are found near the rotor plane and at off design conditions where the blades are stalled or where the rotor operates close to the turbulent wake state
- A good correlation is found between the bound vortex strength as derived from pressure measurements at 82% span and the tip vortex

- strength derived from the PIV measurements
- A large non-uniformity has been found in the flow in the rotor plane due to the passage of the bound vortex. Opposite to expectations the flow at 92% span seems (slightly) more uniform than the flow at 80% span.
- The tip vortex trajectories in yaw differ significantly between the upwind and downwind side of the rotor plane. These differences have a large impact on the axial velocity decays.

Within IEA Task 29 Mexnext many of the discussed measurements cases will be simulated with very different types of models. The results from these calculations are expected to provide additional insights into the above mentioned phenomena. Furthermore new experiments on the same model can hopefully be performed in the future where amongst other things the enhanced PIV capabilities at DNW (a much larger part of the flow field can be covered in a much more efficient way) can provide useful new information.

References

- [1] J.G. Schepers et al. "Verification of European Wind Turbine Design Codes, VEWTDC". In *Proceedings of European Wind Energy Conference, EWEC*, Copenhagen, July 2001.
- [2] S. Schreck. "IEA Wind Annex XX: HAWT Aerodynamics and Models from Wind Tunnel Measurements". NREL/TP-500-43508, The National Renewable Energy Laboratory, NREL, December 2008.
- [3] A.K. Kuczaj. Virtual Blade Model Simulations of the Mexico experiment. NRG-21810/09.97106, NRG Petten, the Netherlands, November 2009.
- [4] H. Snel, J.G. Schepers and B. Montgomerie. "The Mexico project (Model experiments in controlled condition). The database and first results of data processing and interpretation". In Proceedings of EAWE conference The Science of Making Torque from the Wind, August 2007.
- [5] H. Snel, J.G. Schepers and A. Siccama. "Mexico, the database and results of data processing and analysis". In 47th AIAA Aerospace Sciences meeting, January 2009.
- [6] E.T.G. Bot. "Blade Optimisation Tool, User Manual". ECN-E –06-006, Energy Research Centre of the Netherlands, ECN, August 2006.
- [7] H. Snel and J.G. Schepers. "JOULE1: Joint investigation of Dynamic Inflow Effects and Implementation of an Engineering Method". ECN-C-94-107, Energy Research Centre of the Netherlands, ECN, December 1994.

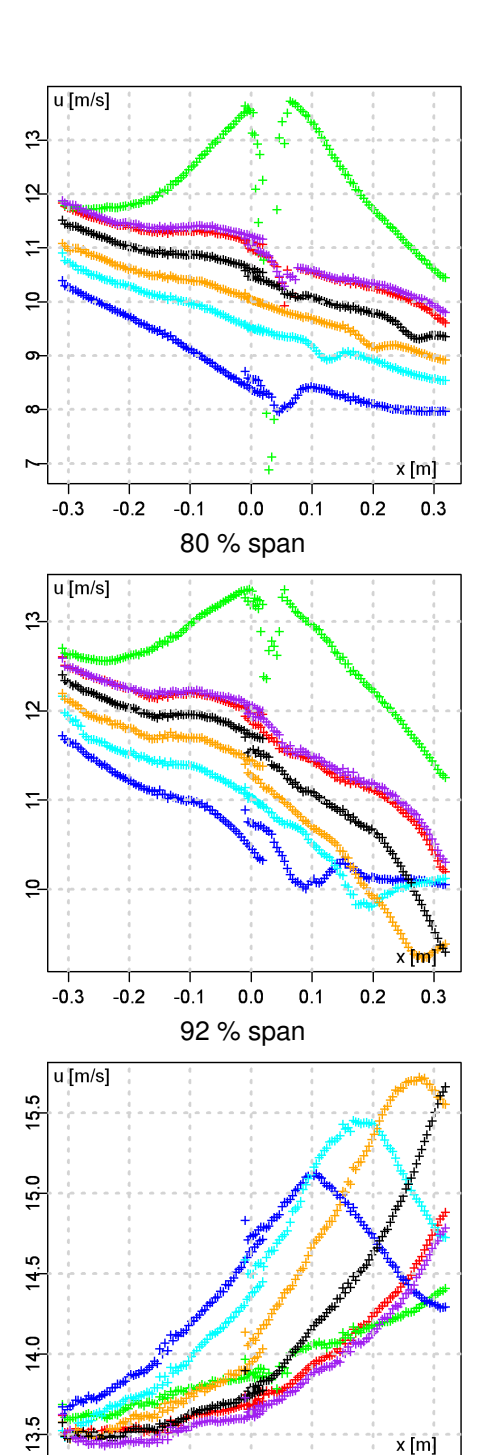


Figure 11: Axial flow traverse for 80%, 92% and 120% span and V =15m/s Different lines represent different blade positions:

0.1

0.2

0.3

-0.3

-0.2

-0.1

0.0

120 % span

$$\Psi=0^\circ$$
 ; $\Psi=20^\circ$; $\Psi=40^\circ$; $\Psi=60^\circ$; $\Psi=80^\circ$;
$$\Psi=100^\circ$$
 ; $\Psi=120^\circ$

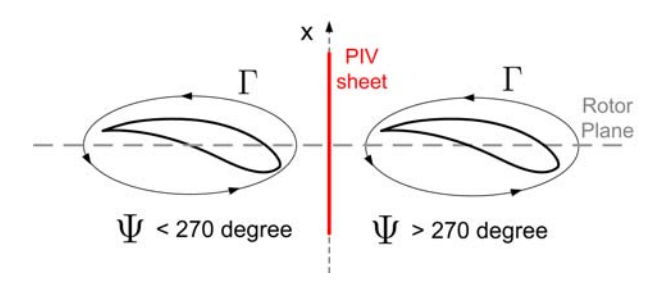


Figure 12: Blade crossing the PIV sheet at 270 degrees azimuth

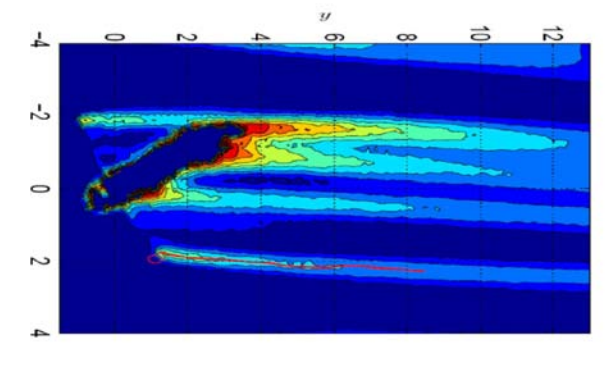


Figure 15: Wake vorticity in yaw as calculated with VBM model of Fluent

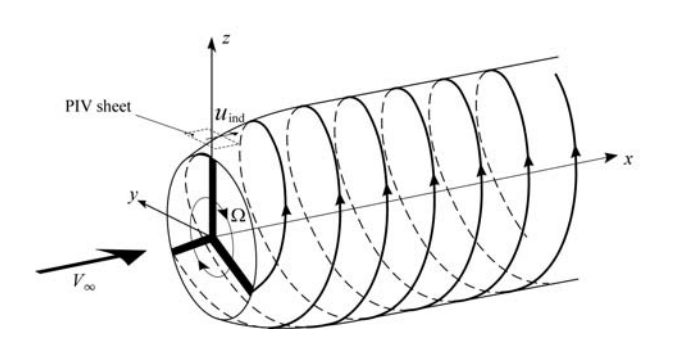


Figure 13: PIV sheet outside helical wake vortex system

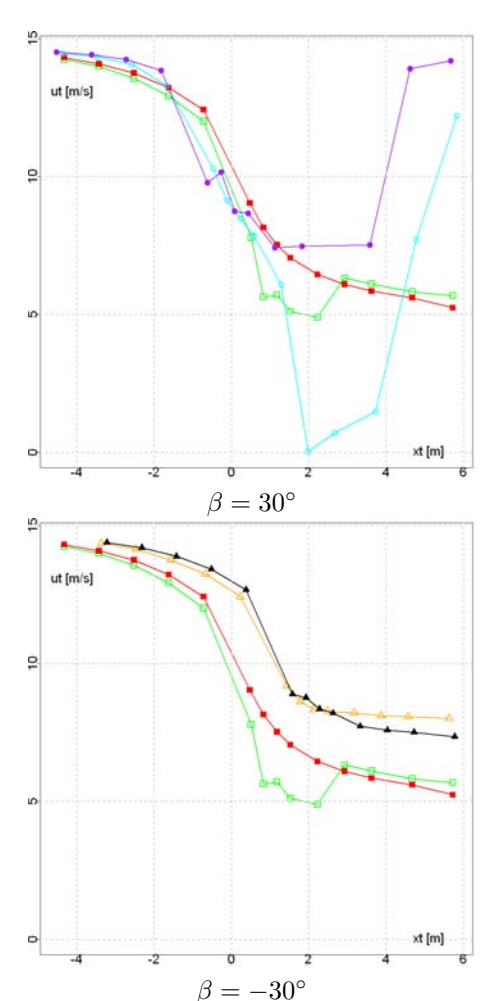
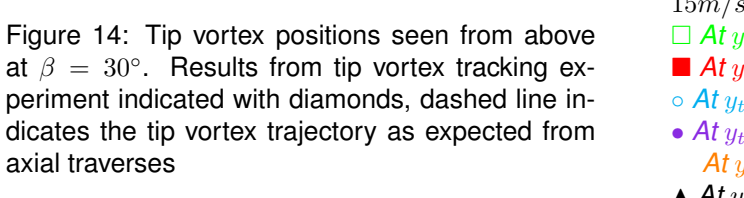


Figure 16: Axial velocity as function of x for $V_{\infty}=15m/s$ and β = 0 and $\pm 30^{\circ}$



```
□ At y_t = -1,374m and \beta = 0^\circ;

■ At y_t = -1,75 m and \beta = 0^\circ;

• At y_t = -1,374m and \beta = 30^\circ;

• At y_t = -1,75m and \beta = 30^\circ;

At y_t = -1,374m and \beta = -30^\circ;

At y_t = -1,75m and \beta = -30^\circ
```